MONITORING VARIABILITY IN 1ES 1959+650 WITH ROVOR

by

Janalee Harrison

A senior thesis submitted to the faculty of

Brigham Young University

in partial fulfillment of the requirements for the degree of

Bachelor of Science

Department of Physics and Astronomy

Brigham Young University

December 2008

BRIGHAM YOUNG UNIVERSITY

DEPARTMENT APPROVAL

of a senior thesis submitted by

Janalee Harrison

This thesis has been reviewed by the research advisor, research coordinator, and department chair and has been found to be satisfactory.

Date	J. Ward Moody, Advisor
Date	Eric Hintz, Research Coordinator
Date	Ross L. Spencer, Chair

ABSTRACT

MONITORING VARIABILITY IN 1ES 1959+650 WITH ROVOR

Janalee Harrison

Department of Physics and Astronomy

Bachelor of Science

Active Galactic Nuclei are galaxy nuclei that emit non-thermal radiation. The standard model describing them assumes the radiation originates from a black hole surrounded by an accretion disk. This model can be tested by measuring how fast the light from the AGN varies. We have constructed and commissioned a 16" telescope named ROVOR (Remote Observatory for Variable Object Research) to monitor AGN light and other variable objects. We report on the first scientifically significant data obtained with ROVOR. For this data we made observations on the blazar 1ES 1959+650 in the Fall of 2008 as part of a multi-wavelength campaign. We discuss how this is compatible with the standard model.

ACKNOWLEDGMENTS

The ROVOR team currently is Dr. J. Ward Moody, Janalee Harrison, Evan Hansen, Richard Pearson, Cameron Pace, and Bret Little. Past team members and supporters are Wes Lifferth, John Ellsworth, Chris Olsen, Aaron Paget, Paul Iverson, Peter Brown, Joe Hopper, Ted Maxwell, Ben Wilson, Jason Gilbert, and Eric Ashbaker. I would like to thank the ROVOR team for working so hard and diligently to get the facility operating. I would also like to thank them for assisting with data acquisition during the observing runs. Thanks to the BYU astronomy group for your support and assistance. Thank you to any one else who may have contributed to ROVOR and subsequent projects. Thank you Alie for helping me with LaTex and my thesis.

Contents

List of Figures

Chapter 1

AGNs

1.1 Introduction to AGNs

Most observable objects do not vary significantly in brightness; but a few do, such as variable stars, tumbling asteroids, lensed stars, and various objects grouped together as active galactic nuclei (AGN). Discovering any variability in an object is important because of the information that can be learned about the object. For instance, the variability of star light reveals information about the star's orbital and rotational periods. The intensity and spectroscopic data of the star's light discloses temperature and chemical composition, from which knowledge of stellar evolution is determined. Tumbling asteroids vary because of the object's motion, surface reflectivity, and chemistry. Lensed stars provide compelling evidence for dark matter and provide information about the make-up and distribution of the galactic halo. By studying AGN variability, we learn about the environment of galactic nuclei, energy transformation mechanisms, and properties of the accretion disk. Active nuclei are generally very bright and far enough away that optically resolving any detail is impossible. Therefore the structure and mechanics of galactic nuclei must be inferred

from the light emanating from the region. We can derive information about the environment from the variability. This thesis discusses the variability of AGNs.

1.2 Types of AGNs

Active galactic nuclei include quasars, blazars, Seyfert galaxies, and radio galaxies. Quasi-stellar radio sources and quasi-stellar objects combine to make the group of AGN called quasars. Quasars have huge redshifts and broad emission lines in their spectra. The redshift is a result of the extreme distance to the object. Quasars were originally thought to be stars because of their intense point-like source of light. However, the emission lines found in the spectra cannot be created by a star and are actually consistent with the spectra seen in most galaxies. Faint "fuzz" was later observed around these objects, providing the optical evidence that quasars are the center of galaxies but are so bright they tend to wash out other features. Radio-loud quasars are noted for their intense source of both light and radio waves and tend to be located at the center of extremely distant elliptical galaxies. Radio-quiet quasars have an intense light source but have weak radio emissions. Their redshifts place them at great distances, but they tend to be nearer than radio-loud quasars and are found more often at the center of spiral galaxies but are also found in ellipticals. [1]

Blazars are also known as BL Lac objects named after the first of this type observed. Similar to quasars, blazars were thought to be super-luminous, highly variable stars but were instead found to reside in the center of very distant elliptical galaxies. Blazars have strong radio emissions, but their nuclei lack absorption and emission lines in the spectrum. The light emitted from the nucleus of a blazar is polarized with a featureless, nonthermal spectrum typical of synchrotron radiation. [2]

Seyfert galaxies are spiral galaxies with very bright compact nuclei that show signs

of intense violent activity. There are two types of Seyferts. Type 1 have both broad permitted emission lines and narrow forbidden lines in their spectra. Type 2 have only narrow emission lines with the widths of the permitted lines being the same as the forbidden lines. [3] With their weak radio emissions, Seyferts are similar to radio-quiet quasars, but are much closer and are not as luminous. Seyferts emit a combination of stellar, nonthermal, and infrared radiation. The luminosity of Seyferts can vary drastically over a span of a few days to a few months. [2]

Radio galaxies are found in ellipticals and are similar to radio-loud quasars except that the nuclei are not as luminous in optical wavelengths. The light emitting from the nuclei of radio galaxies is thermal radiation. There are two types of radio galaxies. Compact radio galaxies have radio emission equal to or smaller than the optical image. Extended radio galaxies have radio emission larger than the optical image often showing two symmetric lobes or jets. Light from the jets is nonthermal synchrotron radiation. [2]

All types of AGN have the common feature of variability. They differ in the amount and the occurrence of the variability. The feature that distinguishes between types is the width of emission lines in the spectra. Emission lines are only created in hot diffuse gases when electrons make transitions to lower orbits by emitting a photon. [3] This feature gives a clue into the environment of AGNs. Many AGN also emit synchrotron radiation which is produced when relativistic electrons travel in a strong magnetic field. [3] Current AGN research is aimed at discovering what environment can cause the energy output, the variability, and the gravitational effects we observe in these objects. The standard model explaining AGNs is a supermassive black hole surrounded by an accretion disk. Observing the accretion disk at different angles explains the different types of AGN that we see.

1.3 The Standard Unified Model

The evidence supporting the standard model is determined as follows. Observations of galaxies show a higher concentration of light in the central bulge or galactic nucleus of most galaxies. The Doppler shifts from light on each side of the galaxy reveals rotational speeds and directions of the material. When Doppler shifts are obtained to within a few hundred parsecs of the nuclei we often see large motion that can only be explained by the presence of a supermassive black hole. [4] By using Newton's forms of Kepler's laws, we get the mass of the object. Because of the gravitational effects taking place, the mass must be concentrated at the center of the galaxy. [1]

The rapid variability seen in AGNs suggests that the central object must also be very small despite its large mass. This size limit comes from the fact that light cannot vary in brightness faster than the light can travel across the object. If the object gives off a sudden flash of light, we see a gradual increase because the flash is stretched out over an interval equal to the difference in light travel time between the nearest and the farthest observable areas of the object. The rapid flicker that we see in AGNs suggests that the variability comes from a small region. The large mass and small volume suggested by observations makes compelling evidence that a black hole must reside in the center of these galaxies. [1]

Supermassive black holes have masses between 10^6 and 10^8 solar masses contained in a relatively small volume with a Schwarzschild radius on the order of $30x10^9$ meters. The strong gravity of the black hole attracts material which spirals in towards the event horizon of the singularity. As this material rotates around the black hole, the material closer to the event horizon moves faster than material farther away, creating friction between particles. The friction heats up the material and ionizes it, which creates the environment needed to observe emission lines in the spectra. The broad

widths of the emission lines indicate that individual light-emitting gas clouds move within the accretion disk at high speeds. Some clouds are moving toward us emitting light with shorter wavelength and higher frequencies, while other clouds are moving away emitting light with longer wavelengths and lower frequencies, resulting in broad emission lines. [1]

As the accretion disk rotates, the friction and magnetic forces within the disk cause particles to lose energy and spiral in toward the black hole. While the gas moves inward within the accretion disk, it gets compressed and heated to very high temperatures. This makes the accretion disk radiate and produce the high luminosity of AGNs across the spectrum. Variations in density and distribution of gases in the accretion disk create some variability. There is a natural limit to the luminosity radiated by material accreting onto a black hole. The Eddington limit is reached when the radiation pressure, produced by the photons emitted by the infalling material, stream outward and push on the material of the accretion disk forcing them back from their inward motion. Without material falling into the black hole, the luminosity decreases and the radiation pressure drops until material can again fall into the black hole. As material falls in, the radiation pressure rises until it reaches the Eddington limit again. This creates a pattern which causes extreme variability. The Eddington limit can be used to determine the mass of a black hole via the equation L_{edd}=$30,000(\mathrm{M}/M_{\odot})L_{\odot}$. [1]

As matter spirals in toward the black hole, it accelerates to supersonic speeds. The material in the accretion disk moves in towards the center as well as rotating around it. Objects that are rotating tend to expand. Because the accretion disk obeys the law of conservation of angular momentum the inward motion stops abruptly near the black hole. The inward motion of material in the accretion disk stops where the tendency to expand out balances the inward pull of the black hole's gravity. The

sudden halt of material spiraling in at supersonic speeds creates shock waves. Which Define the inner edge of the accretion disk. Because of this edge, very little infalling matter reaches the black hole. Part of the matter gets concentrated in high speed orbits close to the hole. Only a fraction of the material in the disk can cross the inner edge and fall into the black hole. This causes a crowding of hot gases near the event horizon, making pressures climb rapidly. To relieve the great pressures and congestion in the inner disk, matter gets expelled at relativistic speeds and escapes the gravitational pull of the black hole. This matter escapes at right angles to the plane of the accretion disk. The magnetic forces then steer the fast moving particles into jets. [1]

Magnetic forces are created in the accretion disk from hot gas that gets ionized to form plasma. The rotational motions of the plasma create magnetic fields. As the plasma rotates around the black hole, it pulls the magnetic field along with it. Because the inner part of the disk rotates faster than the outer disk, the magnetic field lines get twisted to form two helical shapes, one out each side of the plane of the accretion disk. The escaping particles follow the helical magnetic lines, which focus the stream into jets oriented perpendicular to the plane of the accretion disk. [1]

If the accretion disk were observed at different angles, we would see the different types of AGN. For instance, if we observe straight along the jet the observations would be dominated by synchrotron radiation, and there would be no emission or absorption lines. Viewed at this angle we see a blazar. If the jet and disk were both viewed at an angle between 10^o and 80^o, the observer would see broadened spectral lines, intense thermal radiation, and synchrotron radiation. This is the orientation of the radio-loud quasars. It is possible for the standard model to lack jets. If this is the case, observations would lack synchrotron radiation and observers would see a radio-quiet quasar. With the line of sight oriented edge-on, the jets would be visible

from the side, and the observer would see synchrotron radiation. Looking at the disk edge-on, dust and gas obscure the accretion disk, so the emission lines are narrow. From this angle, seeing narrow emission lines and synchrotron radiation, the object would be a radio galaxy. As the material in the accretion disk gets used up by the black hole and depleted, the luminosity will dim and instead of a quasar we would see a Seyfert galaxy. [1]

Chapter 2

ROVOR and Data Acquisition

2.1 ROVOR

ROVOR stands for Remote Observatory for Variable Object Research. The observatory is located outside Delta, Utah at latitude 39^o 27' 17.1" and longitude 112^o 43' 1". ROVOR is a unique, low maintenance facility designed for automated control. Although, the observatory is not yet fully automated, it can be remotely controlled using facilities located at Brigham Young University in Provo, Utah. The telescope will be used mainly for variably object research specifically monitoring AGNs. The ROVOR observatory is designed to work from a target list; which can be interrupted to allow the system to obtain impromptu data on limited opportunity targets such as supernovae and gamma-ray bursts.

The facility is comprised of a 16" telescope located in a specially designed Lifferth Dome. The Lifferth Dome is named after designer, constructor and ROVOR team member Wes Lifferth, full-time staff member at BYU. The Lifferth Dome is a pull-off roof designed for small telescopes and other observational equipment. See Fig. 2.1. It was specifically designed for the needs of the ROVOR project. The roof itself is

Figure 2.1 The main building is nicknamed the dog house and the smaller structure with the satellite dish is nicknamed the out house.

completely removed from the observatory housing walls and cranked off to the side below the optical horizon. This is done using two swing arms on either side of the observatory that work in unison to lift the roof off the structure and rotate down and away into a cleared location. The torque is provided by a threaded rod connected to an electric motor at the back of the building. As the motor rotates, the threads turn through a threaded sleeve connected directly to the support arms. The dome was constructed on BYU campus and installed at its current site in the Fall of 2006. [5]

The telescope is a 16" RC Optical Carbon Truss Ritchey-Chretien with a f/8.4

Figure 2.2 This is a picture taken of the telescope shortly after installation.

focal ratio. The telescope is mounted on a ParamountME base. The telescope is pointed using The Sky software. The telescope was placed in the facility during the summer of 2008. See Fig. 2.2. Data is captured with an Apogee AP47p Marconi CCD47-10 CCD camera controlled with CCDSoft software. For specifications on the CCD see Table 2.1. The filter wheel contains standard Bessel BVRI filters.

Table 2.1. CCD Specifications

Array Size (pixels)	1024x1024
Pixel Size	13x13 microns
Chip Size	13.3 mm x 13.3 mm
Plate Scale	.785 arcsec/pix

2.2 Data Acquisition, Reduction and Photometry

2.2.1 Data Acquisition

Data is recorded with a charge-coupled device (CCD). A CCD is comprised of pixels that collect photons as they strike the chip. The photons are converted into electrons that are stored in each pixel well. The number of electrons in each well is related to the amount of light absorbed. The electron counts are then used to create the digital image. However, the raw images coming from the CCD do not accurately measure the amount of light hitting the frame. [6] Each digital image is filled with noise which must be removed during the reduction process.

2.2.2 Reductions

There are three different types of noise that must be removed from the frames before useful information can be extracted. The first level of noise is caused by the detection of electrons when the electronics are turned on. Each pixel will have a different residual level that must be subtracted from the other calibration frames and the object frames to provide a common zero point. To measure the residual levels, we take images using a zero second exposure time. These images are called bias or zero frames. See Fig. 2.3 for an image of a zero frame.

The second level of noise is due to electrical currents in the equipment that cause the CCD to register electrons not created by photons. To correct for this, we record images with the shutter closed so no light hits the CCD and the only electrons registered are noise. We use the same exposure time as for our object frames because the number of extra electrons the CCD registers depends on the length of the exposure. These calibration frames are called dark frames and are subtracted from the last type of calibration frames and the object frames. Fig. 2.3 has an image of a dark frame.

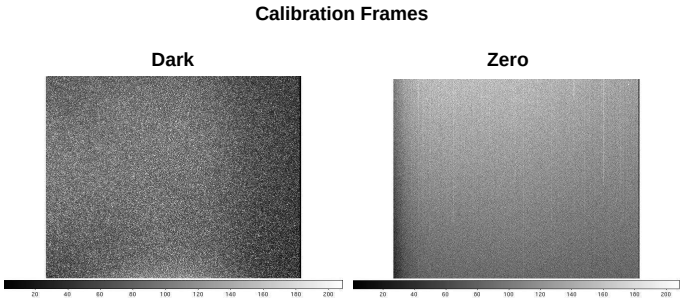

Figure 2.3 Calibration Frame images of a Dark and a Zero. These images were taken at ROVOR October of 2008.

The third type of noise is due to the unequal sensitivity of each pixel and causes an unequal absorption of photons. To account for this, we take short exposures of a uniformly bright and colored area. These images, called flat frames, are scaled to an average of one and divided out of the object frame. [6] Flat frames are taken for each filter type. For the ROVOR data we took both twilight sky flats in the B,V, and R filters as well as flats taken with a white sheet wrapped around the telescope to provide uniform illumination. For the reductions of 1ES 1959+650 the sheet flats were used instead of the sky flats because they turned out to be better frames. See Fig. 2.4 for a comparison of the images.

The files coming from the CCD contain both the image and a header. The header contains details about each frame, such as when it was recorded and the exposure length. We use a program called Image Reduction and Analysis Facility (IRAF) to reduce our images. Before applying the calibration frames to the images, the headers are edited to include the object, the airmass, the filter, the Julian Date, and the

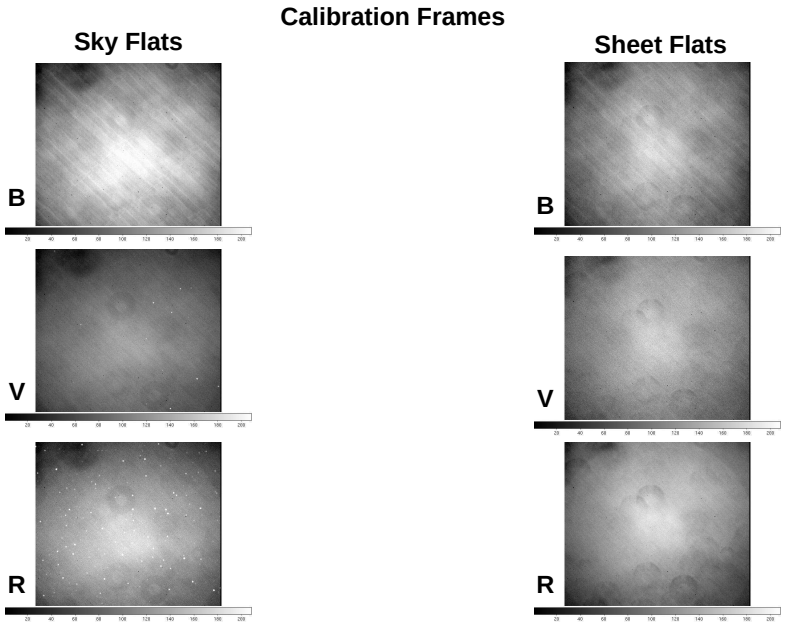

Figure 2.4 This is a comparison of the sky flats to the sheet flats. These images were taken at ROVOR October 17, 2008.

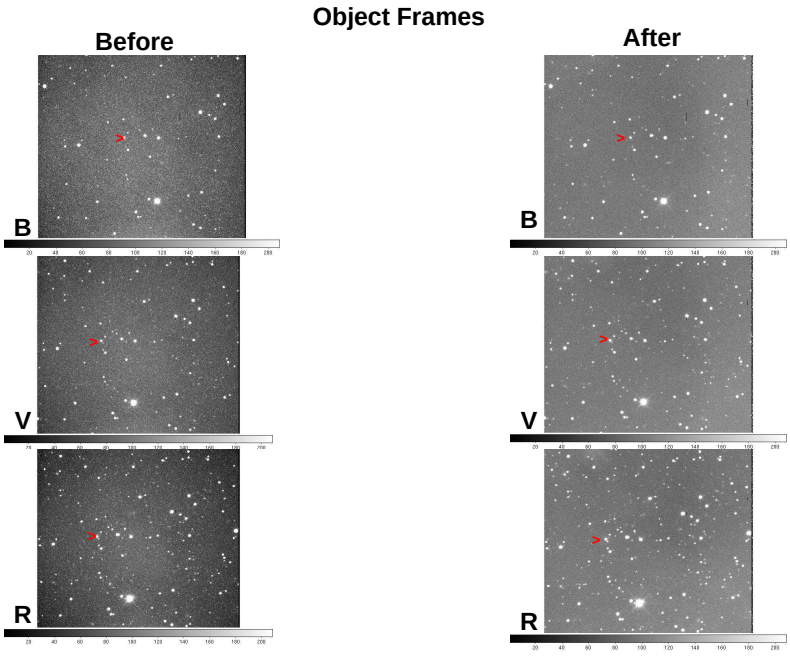

Figure 2.5 This is a comparison of the object frames in each filter before and after reductions. These images were taken with ROVOR October 10,2008. The target is marked with a red arrow.

observatory information. The calibration frame headers were also edited to include the type of frame and the filter. To apply the calibration frames to the images, all of the zero frames were combined into a master zero frame. This was then used to correct the dark frames. The corrected dark frames where then combined into a master dark frame. Both the master dark frame and the master zero frame were used to correct the flat frames. The corrected flat frames were combined into a master flat frame. All three of the master frames were used to correct the object frames. [6] See Fig. 2.5 for a comparison of the object frames before and after the images were reduced.

2.2.3 Photometry

In order to find the magnitude of several objects on a frame, we use a method called aperture photometry. Two circles are drawn centered on each star. The inner circle includes the object and totals the number of counts for the object and the sky. Partial pixel counts are calculated by what fraction of the pixel lies within the circle. The outer circle totals the number of counts between the two circles, which is called the sky count. The sky count is then subtracted from the counts within the inner circle to obtain the total counts for just the object. The counts are then converted into an instrumental magnitude for each object. [6] For Blazar 1ES 1959+650 we treated the target as a point source and did normal aperture photometry on it and the standard stars.

There are many things that affect the light measured from a given object, atmospheric conditions being one of the most important factors. The atmosphere scatters light and the more atmosphere the light has to travel through, the more it scatters. Astronomers use a unit called airmass to measure how thick the atmosphere is. One airmass corresponds to directly overhead; it is the smallest airmass possible. Data becomes unreliable when the airmass exceeds two, which occurs when looking within 30^o of the horizon. Fluctuations in the atmosphere cause light to bend which prevents some of the light from reaching the telescope and causes the object to look dimmer than it really is. This also spreads the light over a greater area on the CCD. Because of this, the magnitudes we get from aperture photometry are not true apparent magnitudes and vary from frame to frame during the night, and differ from night to night. To compensate for this, we use a method called differential photometry. Within each of our frames, there are at least two reported constant stars; stars whose brightness do not vary. We average the instrumental magnitude of the standard stars and then subtract that magnitude from the magnitude of the target object. This difference is

called the differential magnitude of the object and any variations in magnitude that remain are created by the object itself. [6]

2.3 Presentation and Explanation of Data

2.3.1 Background Information on target 1ES 1959+650

Blazar 1ES 1959+650 has been the subject of many multi-wavelength campaigns. This is a bright source that typically flares in the x-ray and VHE gamma-ray bands. It was discovered in the radio band as part of a 4.85 GHz survey performed with the 91m NRAO Green Bank telescope in 1991. In the optical bands it is highly variable and shows structures consistent with an elliptical galaxy. The mass of the central black hole has been estimated to be between 1.3 and 4.4 x 10^8 solar masses. The blazar has been observed to flare in the gamma-ray but not the x-ray. X-rays tend to be higher when the optical bands are brighter. Consequently these results continue to make the target an interesting object to observe. [8]

2.3.2 Data and Explanation of Results

Data for target 1ES 1959+650 was taken with ROVOR nine nights between the 10th and 29th of October 2008 as part of a multi-wavelength campaign. Data was taken in the B,V, and R filters. The frames under went reductions, and aperture and differential photometry as described above. Fig. 2.6 [7] lists the standard stars we used for comparison, their magnitudes in the V and R filters, as well as their location in the field of view.

In appendix A there is a table which lists all frames taken during the 2 week campaign along with filter information and exposure length. All dates in the table

1959+650 (1ES 1959+650)

Coordinates
α= 19:59:59.8522 δ= +65:08:54.668 (2000)
z = 0.047

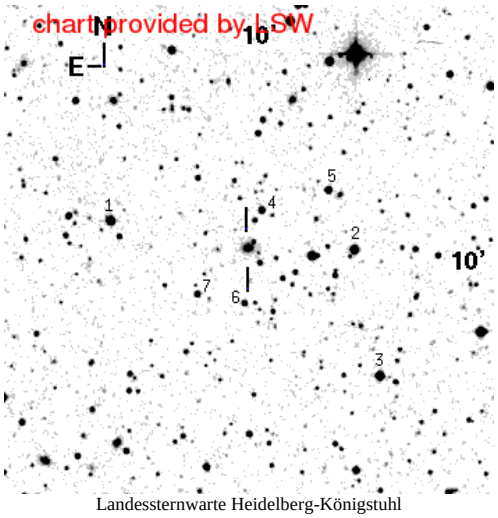

Landessternwarte Heidelberg-Königstuhl

Comparison stars

star	U	B	V	R	I
1			12.67(0.04)	12.29(0.02)	
2			12.86(0.02)	12.53(0.02)	
3			13.18(0.02)	12.27(0.02)	
4			14.53(0.03)	14.08(0.03)	
5			14.54(0.03)	14.00(0.02)	
6			15.20(0.03)	14.78(0.03)	
7			15.24(0.03)	14.79(0.03)	

comparison stars from Villata M. et al., 1998, A&AS 130, 305

Field of view is 10'x10'

Figure 2.6 This figure list the comparison stars used, their magnitudes, and marks their location in the frame.

are in the month of October of 2008. Due to problems during the data acquisition and/or reduction process several frames needed to be discarded to prevent the data from being inaccurate. On the 17th of October frame R-2 was deleted because the exposure length was not long enough. On the 18th of October frame R-2 has a streak across the frame very near the target, possibly from a satellite. This may have affected the photometry, however, we kept the data from this frame in our final results. On the 21st all frames taken in the B filter have strange wavy streaks that appeared after reductions but do not appear in any of the object frames or calibration frames. The possible problem is that these frames were not actually taken in the B filter. The filter wheel is changed by telling the computer which filter to move to. For ROVOR filter 2 is the B filter. The computer takes the filter information for the header of the frame from a different location and the B filter is filter 1 in this location. Because the filter information must be set in two places it creates the possibility of incorrectly labeling the header. If the frame was reduced using a flat not corresponding to the same filter the object was taken in, it could explain the strange pattern that appeared on these frames. Because the photon counts for the target and standard stars were approximately the same as other B frames from other nights we kept these frames in our final results but they could be creating an error in the results.

On the 23rd of October frame R-1 was removed because the exposure length was too short. The last frame removed from the final results was taken on the 29th of October. In the V-4 frame on this night every star in the field has a comet like tail. The streaks or tails behind every star appear on one side of the targets and streak in the same direction for all targets. I do not believe this is a tracking problem with the telescope because the stars themselves are not blurred or streaked and remain solid circles on the frame. I also do not believe it to be a cause of over exposure because even the faintest stars on the frame have it and the tail cuts diagonally across the

CCD columns and could not be the cause of bleeding over into neighboring wells. This frame was discarded because of this and the reason behind the tails remains unknown and have not been repeated in any other frames.

There are other possible reasons for errors made during the reduction process. Because the dark frames must be exposed for the same length as the object frames, it is possible that the darks used to reduce some frames were not at the same exposure length.

After the frames were reduced and the aperture photometry was finished the target object and standard stars' magnitudes were placed in an excel worksheet. Within excel I used the standard stars to adjust the magnitudes for the target to the differential magnitude. Fig. 2.7 is a graph of the apparent magnitude of the target object versus the heliocentric Julian date (HJD), Fig. 2.8 and Fig. 2.9 are graphs of the first two standard stars apparent magnitudes versus the HJD and Fig. 2.10 is a graph of the adjusted magnitude of the target versus the HJD. By plotting the magnitudes versus the HJD we can see how the object varies in time. From figures 2.7, 2.8, and 2.9 you can see that any variability of the magnitude of the target object during the time period follows the same pattern of variability of the two standard stars. Referring back to figure 2.6 you can see we only have published magnitudes for the standard stars in the V and R filters to compare the ROVOR data to. Therefore, I only adjusted the R and V filters for the target frame. From figure 2.10 you can see that the target object did not vary significantly in the V and R filters once adjustments were made to the differential magnitude.

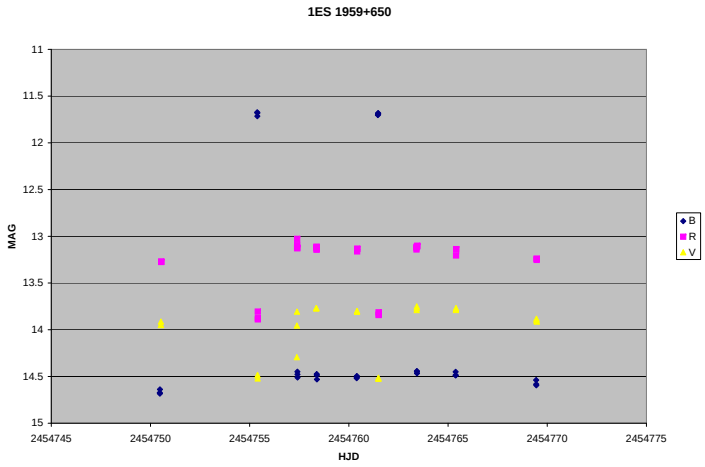

Figure 2.7 This is a graph of the apparent magnitudes for target 1ES 1959+650 vs. the HJD. The magnitudes do not change much in the two week period.

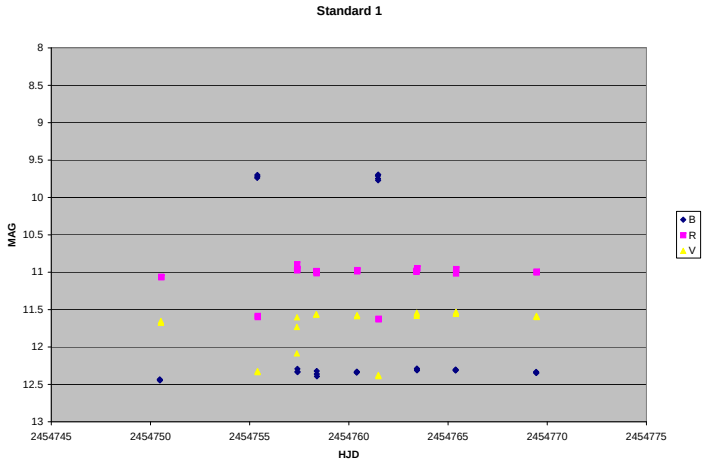

Figure 2.8 These are graphs of the apparent magnitudes for standard stars 1 vs. the HJD.

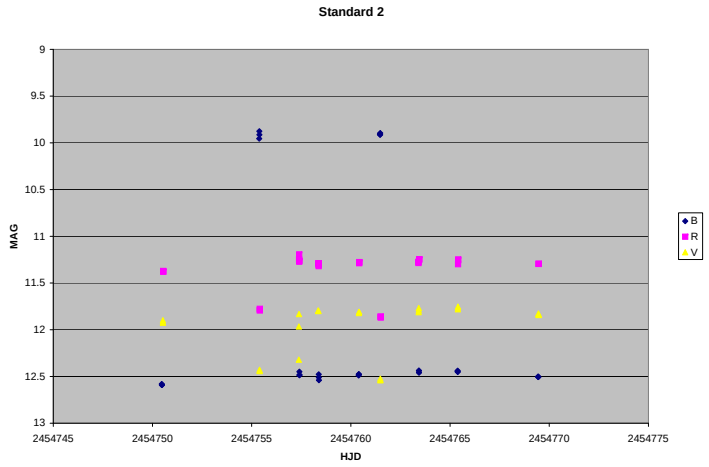

Figure 2.9 These are graphs of the apparent magnitudes for standard stars 2 vs. the HJD.

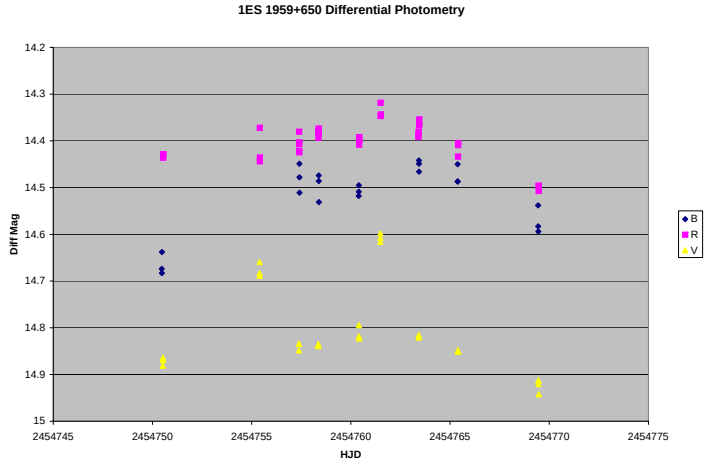

Figure 2.10 This is a graph of the differential magnitudes for target 1ES 1959+650 vs. the HJD. The magnitudes do not change much in the two week period.

2.4 Conclusion

The data taken for the multi-wavelength campaign during October of 2008 was ROVOR's maiden observing run. The data in appendix A is the first scientific data this telescope has taken. Part of this project was to determine if the telescope can be used for its intended purpose and give accurate results. Because this data is part of a campaign it has been and will be shared with the other contributing parties to the campaign. We can take data from other campaign members and compare it to our own. Table 2.2 lists the HJD and differential magnitudes for the target in the R filter. The data in this table is from ROVOR and was reduced for this thesis in IRAF as explained in the previous sections. Table 2.3 is the same data taken with ROVOR except it was reduced by campaign contributor Dr. Alberto Sadun at the University of Colorado, Denver using a program called MIRA instead of IRAF. Also in this table we list the magnitudes from the IRAF reductions with the standard deviation for comparison. Finally, Table 2.4 contains results from campaign contributors in New Mexico taken with their own telescope. The magnitudes in all three tables are all from the R filter. The magnitudes in all three tables are very similar. ROVOR's data is closest to New Mexico's data in magnitude and deviation. This provides us with the evidence we need to know for sure that ROVOR can be professionally used to provide scientifically accurate data on variable objects such as AGN. The comparison in table 2.3 of the MIRA reductions verses the IRAF reductions shows that IRAF reductions were more accurate. The difference in results may come from the aperture used for the photometry. Target 1ES 1959+650 has another object in close proximity and an aperture too large would include the neighboring object and give inaccurate magnitudes for the target. We treated the target as a point source but it is an extended object. Another problem with the photometry that could be occurring is the

point spread function is wider then what we look at and we may be cutting it too close. ROVOR and the reduction methods still needs some adjustments to be able to get more accurate results.

The Data gathered on blazar 1ES 1959+650 with ROVOR do not vary with any significance in the B, V, and R wavelengths. The blazar was "quiet" in the optical during the data acquisition period. We can not conclude much about the nature of the blazar with these results. However, this data is valuable for being combined with similar data from previous and for future observations. It is also important when combined with the other wavelengths of the multi-wavelength campaign. Historically 1ES 1959+650 has seen most of its variability in the x-ray and gamma-ray wavelengths of the electromagnetic spectrum and being stable in the optical for the short time period the target was observed is not surprising. Further observations on the target are necessary to learn possible reasons why the AGN has periods of little or no optical variability.

Table 2.2. ROVOR data, IRAF reductions

HJD	R Magnitude
2454750.53797462	14.43243
2454750.54213768	14.43600
2454750.54658246	14.42857
2454755.40858636	14.37200
2454755.41252707	14.44386
2454755.41646559	14.43571
2454757.38977641	14.42157
2454757.39296805	14.38043
2454757.39616630	14.40329
2454757.39871582	14.40700
2454757.40126603	14.42457
2454758.36656651	14.39371
2454758.36917864	14.38171
2454758.37178568	14.37914
2454758.37439330	14.38386
2454758.37700081	14.37371
2454760.41902250	14.40814
2454760.42161634	14.39200
2454760.42421019	14.39829
2454761.49823193	14.31843
2454761.50287310	14.34686
2454761.50684459	14.34357
2454763.40652044	14.38757
2454763.40907216	14.38043
2454763.41161658	14.39186
2454763.44111620	14.36557
2454763.44505298	14.36686
2454763.44899808	14.35414
2454765.40460712	14.43371
2454765.40719402	14.40471
2454765.40977652	14.40914

Table 2.3. ROVOR Data, MIRA reductions

HJD	R Magnitude	IRAF	standard deviation
2454750.536775	14.492	14.43233	±.003716
2454757.394360	14.467	14.40737	±.017607
2454758.365411	14.456	14.38243	±.007360
2454760.417882	14.451	14.39948	±.008135
2454763.443937	14.454	14.37441	±.014560
2454765.408679	14.428	14.41585	±.015622

Table 2.4. New Mexico data

HJD	R Magnitude
2454741.647396	14.595
2454743.635093	14.537
2454749.633681	14.516
2454752.625347	14.550
2454756.659120	14.405
2454758.625729	14.385
2454759.670926	14.388
2454760.629681	14.382
2454762.683044	14.371
2454765.624387	14.393
2454768.613275	14.399
2454770.611285	14.440
2454779.702373	14.622

Bibliography

[1] R. A. Freedman, W. J. Kaufmann III, *Universe*, 8th ed. (New York, New York, 2008), pp. 669-687.

[2] M. Zielik, S. A. Gregory, *Introductory Astronomy and Astrophysics*, 4th ed. (New York, New York, 1998), pp. 465-485.

[3] B. W. Carroll, D. A. Ostlie, *An Introduction to Modern Astrophysics*, (Reading, Massachusetts, 1996), pp. 1155-1214.

[4] J. Kormendy, D. Richstone, "Inward Bound–The Search for Supermassive Black Holes in Galactic Nuclei," Annual Review of Astronomy and Astrophysics **33,** 581–624 (1995)

[5] J. Ward Moody, "ROVOR," http://rovor.byu.edu/rovor-info.php (Accessed December 10, 2008)

[6] N. Porter, "Continued Observations of the Variable Star V577 Ophiuchi, A Binary System with a Delta Scuti Component," (Senior Thesis BYU, 2008)

[7] M. Hauser, "Finding Chart," http://www.lsw.uni-heidelberg.de/projects/extragalactic/charts/1959+650.html (Accessed December 12, 2008)

[8] G. Tagliaferri, et. al, "Simultaneous Multiwavelength Observations of the Blazar 1ES 1959+650 at a Low TeV Flux," http://www.journals.uchicago.edu/doi/pdf/10.1086/586731 (Accessed December 10, 2008)

Appendix A

Data Table

This section has a complete table of the data taken during the two week observing run as part of the multiwavelength campaign on blazar 1ES 1959+650. See Table A.1. All dates in the table are in the month of October of 2008. Observations were taken between sunset and midnight on the date listed in the table. The table also lists the filter and frame number as well as the exposure length in seconds.

Table A.1. Summary of Data

Date	Filter and Frame Number	Exposure length in seconds
10th	B 1	300
	B 2	300
	B 3	300
	V 1	300
	V 2	300
	V 3	300
	R 1	300
	R 2	300
	R 3	300
15th	B 1	300
	B 2	300
	B 3	300
	V 1	300
	V 2	300
	V 3	300
	R 1	300
	R 2	300
	R 3	300
17th	B 1	300
	B 2	300
	B 3	300
	V 1	300
	V 2	300
	V 3	300
	R 1	300
	R 2	170.625
	R 3	180
	R 4	180
	R 5	180
18th	B 1	300
	B 2	300

Table A.1 (continued)

Date	Filter and Frame Number	Exposure length in seconds
	B 3	300
	V 1	300
	V 2	300
	V 3	300
	R 1	180
	R 2	180
	R 3	180
	R 4	180
	R 5	180
20th	B 1	300
	B 2	300
	B 3	300
	V 1	300
	V 2	300
	V 3	300
	R 1	180
	R 2	180
	R 3	180
21st	B 1	300
	B 2	300
	B 3	300
	B 4	300
	V 1	300
	V 2	300
	V 3	300
	R 1	300
	R 2	300
	R 3	300
23rd	B 1	300
	B 2	300
	B 3	300

Table A.1 (continued)

Date	Filter and Frame Number	Exposure length in seconds
	V 1	300
	V 2	300
	V 3	300
	R 1	300
	R 2	180
	R 3	180
	R 4	180
	R 5	300
	R 6	300
	R 7	300
25th	B 1	300
	B 2	300
	B 3	300
	V 1	300
	V 2	300
	V 3	300
	R 1	180
	R 2	180
	R 3	180
29th	B 1	300
	B 2	300
	B 3	300
	V 1	300
	V 2	300
	V 3	300
	V 4	300
	R 1	180
	R 2	180
	R 3	180